ROYAL SOCIETY
OF CHEMISTRY

PAPER
Bin Yuan *et al.*
Assessment of long tubing in measuring atmospheric
trace gases: applications on tall towers

Check for updates

Assessment of long tubing in measuring atmospheric trace gases: applications on tall towers†

Xiao-Bing Li,‡[ab] Chunsheng Zhang,‡[c] Aiming Liu,[c] Bin Yuan, [ID] *[ab] Honglong Yang,[c] Chanfang Liu,[d] Sihang Wang,[ab] Yibo Huangfu,[ab] Jipeng Qi,[ab] Zhijie Liu,[ab] Xianjun He,[ab] Xin Song,[ab] Yubin Chen,[ab] Yuwen Peng,[ab] Xiaoxiao Zhang,[ab] E. Zheng,[ab] Lei Yang,[ab] Qing Yang,[ab] Guangzhi Qin,[ab] Jun Zhou[ab] and Min Shao[ab]

Perfluoroalkoxy alkane (PFA) Teflon tubing has been widely used to draw air samples for analyzing atmospheric trace gases. However, impacts of long tubing on measurements of atmospheric trace gases have rarely been reported so far, especially for various organic trace gases. In this study, interactions between long tubing and various trace gases were assessed using a combination of laboratory tests, field experiments, and modeling techniques. A tower-based observation system of trace gases was also established using long tubes. The results show that measured concentrations of organic compounds required varying amounts of time (*e.g.*, 10–474 s for a 400 m-long tubing at a flow rate of 13 standard liters per minute) to stabilize after traversing the tubing. Tubing delays of organic compounds were highly dependent on their saturation concentrations and the residence time in the tubing. In laboratory tests, there are no detectable losses of the targeted chemical species after traversing the 400 m-long tubing. In real applications, concentrations of nitric oxide (NO) cannot be well measured through long tubes in the daytime due to its low ambient concentrations and rapid consumption by ozone. Negligible losses were observed for most of the other targeted species when measured using long tubes. Measurements of various trace gases made by the vertical observation system can well characterize their concentrations and vertical distributions. However, the measurements of a trace gas made by the vertical observation system at each altitude cannot be used to interpret its temporal variability at time scales lower than its tubing delay. In addition to their usage on tall towers, long PFA Teflon tubes can be also used on mobile platforms (*e.g.*, tethered balloons) for vertical measurements of atmospheric trace gases or to surveil emissions of targeted chemical species at multiple sites.

Environmental significance

Long tubing has been widely used as inlets for measurements of atmospheric trace gases in certain circumstances, *e.g.* tall towers, balloons, or unmanned aerial vehicles. However, interactions between various trace gases and the long tubing remain unclear so far, which highly limits the development of vertical observations of atmospheric trace gases to a large extent. To address this concern, we systematically investigated the impacts of long tubing on measurements of various trace gases, namely O$_3$, NOx, and a set of organic compounds, using a combination of laboratory tests, field experiments, and modeling techniques. The findings presented here could provide a solid theoretical basis and guidance for the usage of long tubing in analyzing atmospheric trace gases in the future.

[a]Institute for Environmental and Climate Research, Jinan University, Guangzhou 511443, China. E-mail: byuan@jnu.edu.cn

[b]Guangdong-Hongkong-Macau Joint Laboratory of Collaborative Innovation for Environmental Quality, Guangzhou 511443, China

*[c]Shenzhen National Climate Observatory, Shenzhen 518040, China*

[d]Shenzhen Ecological and Environmental Monitoring Center of Guangdong Province, Shenzhen 518049, China

1. Introduction

Greenhouse gases, gaseous pollutants, and precursors of secondary pollutants have notable impacts on both regional air quality and climate change, thus as important trace gases in the lower troposphere.[1–3] Concentrations of these trace gases along with their spatio-temporal variability at ground level have been well characterized so far.[4–6] However, their vertical variations and influential factors are rarely reported due to the difficulty in obtaining direct observations. Knowing vertical structures and key drivers of these trace gases is important for elucidating their
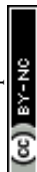
source emission characteristics and roles in regulating climate change and air quality at both regional and global scales.[7–10]

Vertical measurements of atmospheric trace gases in the lower troposphere have been made by a variety of approaches, *e.g.*, sounding and tethered balloons,[11–15] unmanned aerial vehicles (UAVs),[16–18] towers,[19–24] remote sensing techniques,[25–27] and aircraft.[28–32] The advantages and disadvantages of these approaches have been discussed in the literature.[33,34] In summary, towers could provide an economic and flexible way to regularly perform vertical gradient measurements of trace gases, particularly in urban and suburban environments.

Direct deployment of instruments at multiple altitudes of a tower (*in situ* observations) is the most popular way to make regular observations of targeted species.[7,21,35] However, more instruments will be deployed if concentrations of targeted species at more heights are required to be measured simultaneously. The economic costs of the initial establishment and subsequent maintenance of such a tower-based platform are very huge. In addition, some instruments (*e.g.*, many mass spectrometers) are very bulky and may not be directly deployed on a tower, largely limiting the number of gaseous species that could be routinely measured. Instead of *in situ* observations, air samples at multiple heights of a tower could be drawn by long tubes and sequentially analyzed using only one set of instruments deployed at a certain level (most frequently on the ground).[36–39] The most concerning question for this approach was measurement uncertainties of trace gas concentrations, particularly for various organic compounds, caused by the usage of long tubing.

Tubes made of perfluoroalkoxy alkane (PFA), polytetrafluoroethylene (PTFE), and fluorinated ethylene propylene are widely recommended for analyzing organic and inorganic species due to their excellent chemically inert properties.[15,40–43] Previous studies found that the inner walls of these tubing types can interact with air samples by the absorption/desorption of trace gases,[40,44] namely gas–surface interactions. Certain amounts of time are required to reach an equilibrium between the adsorption and desorption, leading to time delays (usually recognized as tubing delays) in measured concentrations of trace gases after traversing the tubing. In addition, molecular diffusion and dispersion (Taylor dispersion) can also induce tubing delays of various trace species.[45] Chemical reactions of reactive trace gases that may occur during the course of transport further increase their measurement uncertainties.[15] For most organic compounds, tubing delays are dependent on their saturation concentration (C^*), tubing size, and tubing flow rate but are independent of species concentration and humidity. For some small polar molecules, tubing delays are dependent on humidity and their Henry's law coefficient. Tubing delays of various organic compounds and inorganic species in these tubing types with short lengths (several or dozens of meters) have been investigated.[40,41,46] Assessment of the long tubing (<200 m) in measuring ambient concentrations of ozone, NOx, and a small set of non-methane hydrocarbons (including seven alkanes and two aromatics) has been also performed in the literature.[14,15,43] However, interactions between much longer tubes (*e.g.*, several hundreds of meters) and more trace gases

(particularly for various organic trace gases) should be also systematically investigated.

In this study, the combination of laboratory tests, model simulations, and field validations was used to systematically assess the impacts of long PFA Teflon tubes on measurements of different trace gases. In addition, a tower-based system was established using long PFA Teflon tubes to make vertical gradient measurements of atmospheric trace gases with high time resolutions. Lastly, the results of a field campaign were discussed to preliminarily reveal the vertical distributions of some typical species.

2. Methods and materials

2.1. Tubing selection and instruments

The residence time of sample gas (Fig. S1†) in a section of the tube, which is defined as the ratio of the tubing length to the inside flow velocity, is inversely proportional to the flow rate. The decrease in residence time could reduce the impacts of the tubing on measurements of trace gases.[44] However, the increase in flow rate can rapidly increase the pressure drop of sample gas (Fig. S2†), which is unfavorable for instruments to draw subsamples from the tubing. Therefore, thick PFA Teflon tubing with an outer diameter (OD) of 1/2″ and an inner diameter (ID) of 0.374″ was used to balance the flow rate, pressure drop, and economic cost. According to the results of our tests, the instruments used in this study can normally work when the flow rate of the sample gas stream in a 400 m long tubing (the longest tube used in this work) was lower than 20 standard liters per minute (SLPM).

The instruments used in this study all have fast response times to capture changes in concentrations of targeted trace gases. Measurements of organic compounds were made using a high time-resolution proton-transfer-reaction quadrupole interface time-of-flight mass spectrometer (PTR-ToF-MS) (Ionicon Analytik, Innsbruck, Austria) that has both the hydronium ion (H_3O^+) and nitric oxide ion (NO^+) chemistry. The PTR-ToF-MS was operated at an E/N ratio of ~120 Td. Other settings and parameters of the PTR-ToF-MS have been described in our previous studies.[46–48] Ozone was measured using the ultraviolet photometry method (49i, Thermo Fisher Scientific Inc., USA; 405, 2B Tech, USA), NOx was measured using the chemiluminescence method (42i, Thermo Fisher Scientific Inc., USA) and the UV absorption method (205, 2B Tech, USA), and H_2O and CO_2 were measured using the nondispersive infrared method (Li-840A, Licor Inc., USA).

2.2. Laboratory tests

Laboratory tests were performed to investigate interactions between long tubes and various trace gases. In brief, the mixture of gas standards (namely ozone, NO, NO_2, CO_2, and a set of organic compounds in Tables S1 and S2†) and zero air ($O_2 + N_2 \geq 99.9995\%$) (Fig. S3–S7†) were added to the tubing at fixed flow rates (6–18 SLPM). Other detailed information on the instruments and the experimental setup is provided in the ESI.† Impacts of long tubing on measurements of trace gases can be

© 2023 The Author(s). Published by the Royal Society of Chemistry

Environ. Sci.: Atmos., 2023, **3**, 506–520 | **507**

quantitatively assessed according to changes in their concentrations measured at the two ends of the tubing. In this study, scatter plots and linear fittings ($y = kx + b$; k is the slope and b is the intercept) were mainly used to perform the comparison
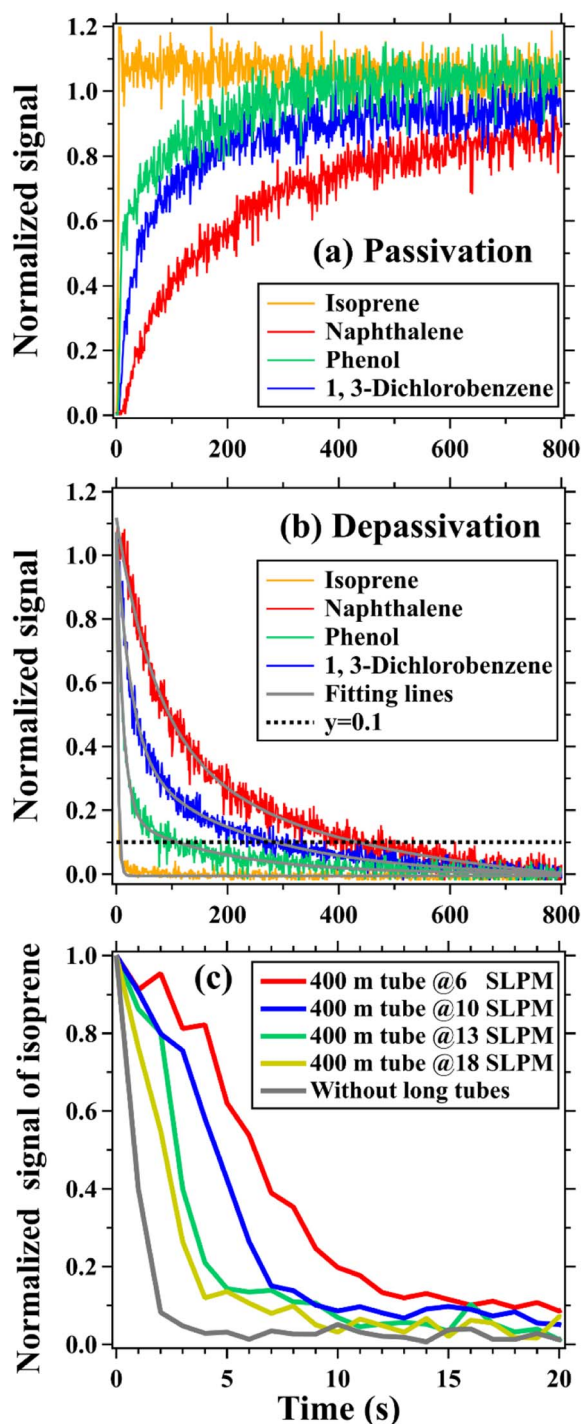

Fig. 1 (a) Passivation and (b) depassivation curves of four selected ion signals measured by PTR-ToF-MS for the 400 m long tubing at a flow rate of 13 SLPM. Ion signals were normalized to those measured at the start time of the step-function change; Grey solid lines in panel (b) are double exponential fittings. (c) Depassivation curves of isoprene for the 400 m long tubing at different flow rates.

analysis. The coefficient of determination, denoted by R^2, was used to evaluate the goodness of fit. Inorganic species, namely ozone, NOx, and CO_2, have small tubing delays (only several seconds) even in a 400 m long tube and thus were not discussed. As validated in previous studies, tubing delays of most organic compounds are independent of concentration and humidity,[49,50] but dependent on $C*$ and tubing size.[40,41,44] Tubing delays of some small polar molecules (e.g., HCl and PAN) are dependent on humidity and Henry's law coefficient.[41] In this study, only tubing delays of the organic compounds measured by PTR-ToF-MS were discussed.

In this study, tubing delays of organic compounds were defined and computed using the same methods in previous studies.[40,41,44] Briefly, the tubing delay of a trace gas is defined as the amount of time required to reach 90% of the change in its concentration before entering the tubing.[40,41,44] It should be noted that the tubing delay is distinct from the residence time as discussed in Section 2.1. For tubing with a fixed length and inside flow rate, all the chemical species have the same residence time but have differentiated tubing delays. Tubing delays of organic compounds were calculated according to the depassivation curves of their ion signals measured at the outlet end of the tubing (Fig. 1 and S8–S10†). Ion signals of organic compounds were first normalized to those measured at the start time of the step-function change at the outlet end of the tubing. Then, the normalized depassivation curves were fitted using the double exponential method, as formulated in eqn (1), to reduce the impacts of the noise in measured ion signals of trace gases. The tubing delay of an organic compound is determined as the time when its double exponential fitting line declined to 0.1, as shown in Fig. 1(b). As shown in Fig. 1(c), the inner parts of the instruments and auxiliary tubes (these tubes have ODs of 1/4″ and 1/8″ and were used to connect instruments and long tubes) used in laboratory tests can also cause delay times for the measurements of organic compounds and should be excluded in the analysis. However, the measured delay times caused by the instruments and auxiliary tubes were much lower than those caused by long tubes, as shown in Fig. S11.† Therefore, the delay times of targeted organic compounds caused by the instruments and auxiliary tubes were directly subtracted from those measured for long tubes.

$$y = y_0 + A_1 \exp\left\{\frac{-(x - x_0)}{\tau_1}\right\} + A_2 \exp\left\{\frac{-(x - x_0)}{\tau_2}\right\} \quad (1)$$

2.3. Field validations

Field validations of long PFA Teflon tubes in measuring concentrations of targeted trace gases were conducted at the base of the Shiyan Meteorology Tower (SMT) in Shenzhen, China.[35,51] The SMT is 365 m high (Fig. S12†) and is located ∼20 km to the northwest of downtown Shenzhen and ∼80 km to the southeast of downtown Guangzhou in the Pearl River Delta region. A vertical observation system was established using PFA Teflon tubes (OD: 1/2″) based on the SMT. Five heights, namely 40, 70, 120, 220, and 335 m, on the SMT (Fig. S13†) were selected to mount inlets of the tubes (Table S5†). At each inlet height,

two tubes were installed with one for backup. Filters (47 mm PFA filter holder; 2 μm PTFE filter membrane) were installed downstream of the tubing inlets (Fig. S12†) to remove fine particles. The inlet ends of the tubes were mounted downward to prevent contamination from precipitation. To prevent photochemical consumption/formation of trace gases, all the tubes were installed inside an iron box and were wrapped with black plastic bellows on the tower to avoid exposure to sunlight. The mixture of zero air and gas standards can be delivered to the inlet height of 120 m using the backup tube, aiming to dynamically assess the impacts of the tubing on measurements of targeted trace gases during field campaigns. An additional inlet, ~5 m above ground level, was mounted on the rooftop of an observation room at the base of the SMT.

All six tubes of the vertical observation system were continuously drawn using a rotary vane vacuum pump during a field campaign. Critical orifices (orifice diameter: 0.063″) were used to control the flow rate of the air sample stream in each tube (Fig. S13†). The six tubes were drawn simultaneously rather than being sequentially drawn so that they can be kept flushing with ambient air to reduce tubing delays of the organic compounds. Subsamples were sequentially drawn by instruments from the six tubes through a Teflon solenoid valve group, which can perform the switch of air sample flow at designated time intervals. As a result, flow rates of air sample streams for the six tubes varied between 12.0 and 15.0 SLPM (Table S5†) without subsampling and were lower than 20 SLPM with subsampling.

A field campaign was conducted in January 2021, during which vertical gradient measurements of various trace gases were made by the vertical observation system. The measurements of organic compounds and CO_2 had time resolutions of 5 s. The PTR-ToF-MS was operated with the first 44 min in the H_3O^+ mode (including three H_3O^+ modes: 16-14-14 min) and the remaining 16 min in the NO^+ mode in one hour. Background measurements of the PTR-ToF-MS were automatically performed in the last 2 min of each mode by passing ambient air through a platinum catalyst to remove organic compounds.[52] The platinum catalyst is immediately in front of the inlet of the PTR-ToF-MS and has no impact on measurements of the other instruments. Automated calibrations with certified gas standards were performed three times daily in the H_3O^+ mode (Table S1†) and twice daily in the NO^+ mode (Table S2†). The measurements of other trace gases, namely ozone, NO/NO_2/NOx, and CO_2, had time resolutions of 10 s during the campaign. In addition to PTR-ToF-MS, background measurements of the other instruments were made once daily using zero air. These instruments were calibrated in our laboratory using a mixture of zero air and respective gas standards before and after the campaign.

As introduced above, all the tubes were continuously flushed with ambient air to minimize the effects of the delay time from the long inlets. Therefore, the selection of switching intervals between the inlet heights should follow two principles: (i) obtaining as many effective samples as possible at each height; (ii) performing as many vertical measurement cycles as possible in a certain amount of time. According to our tests, the measurements of all trace gases made in the first 30 s and the

last 10 s of a switch should be discarded to remove cross interferences from different inlet heights. In this study, the solenoid valve group was set to switch to a new inlet height every two minutes during the field campaign.

In addition to the vertical observation system established by our group, the Shenzhen Environmental Monitoring Center has directly deployed ozone monitors at 60, 110, 210, and 325 m and NOx (NOx and NO) monitors at 70, 120, 220, and 335 m on the SMT.[35] Therefore, the gradient measurements of ozone and NOx made by the observation system can be assessed by comparisons with those directly made on the SMT. As suggested in previous studies,[15,43] ambient air samples were also alternatively measured by using a 5 m and a 400 m long PFA Teflon tube (OD: 1/2″) to further assess the impacts of long tubing on measurements of various trace gases in real environments. This field validation experiment was conducted at the SMT base from LT 17:30 on January 29 to LT 12:30 on January 30, 2021, covering both dark and daylight times. The two tubes were run side by side on the rooftop of the observation room and their switch was performed using a solenoid valve group at time intervals of 4 min.

2.4. Box model simulations

In addition to gas–surface interactions, concentrations of reactive gaseous species (*e.g.*, ozone, NO, and unsaturated hydrocarbons) may change to some extent after traversing the tubing due to chemical formation/consumption. Therefore, a zero-dimensional box model (F0AM) coupled with the Master Chemical Mechanism (v3.3.1)[53,54] was used to assess the impacts of chemical reactions on measurements of targeted trace gases after traversing the tubing.

To investigate the maximum potential losses of targeted gaseous species after traversing the 400 m long tubing, a moment with strong solar radiation and high ozone concentration at LT 14:00 was selected to perform the simulation. The input data of meteorological parameters used the measurements made at an urban site in Guangzhou (23.15° N, 113.36° E), China on October 1, 2018.[46,48] Other settings and parameters of the box model are summarized in Table S6.† A spin-up of 3 h (LT 11:00–14:00) was used to minimize the influences of initial conditions on simulation results. The model was run without inputting data of organic compounds during the spin-up time. At LT 14:00, the mixing ratios of a set of organic compounds (Table S6†) were set to 2 ppb, and the solar radiation was set to zero to reproduce the chemical reactions of various species in the absence of sunlight (Fig. S14†). As shown in Fig. S1,† the residence time of sample gas in the 400 m long tubing is less than 180 s at a flow rate of 13 SLPM. Therefore, chemical losses of targeted chemical species could be characterized by the changes in their concentrations between LT 14:00 and 14:03.

3. Results and discussion

3.1. Tubing delays of various organic compounds

As shown in Fig. 1, concentrations of organic compounds have significant but differentiated delay times after traversing the 400 m long tubing at the flow rate of 13 SLPM. In addition to

© 2023 The Author(s). Published by the Royal Society of Chemistry

Environ. Sci.: Atmos., 2023, **3**, 506–520 | **509**

gas–surface interactions, the longitudinal mixing of trace gases, caused by molecular diffusion and dispersion,[45] can also have effects on their concentrations after traversing long tubing. According to the method (see details in the ESI†) used in the literature,[45] the influence times of molecular diffusion and dispersion, denoted by t_m, on measurements of organic compounds after traversing a tubing can be estimated. Taking isoprene ($C^* = 2.0 \times 10^9$ µg m^{-3}) and chlorobenzene ($C^* = 6.6 \times 10^7$ µg m^{-3}) as examples, the two organic compounds have very significant differences in both saturation concentrations and measured tubing delays, as summarized in Tables S3 and S4.† However, the estimated t_m for isoprene and chlorobenzene has minor differences and all slowly decrease with the increase in flow rate. This is slightly different from the observed results that the measured tubing delays of organic compounds rapidly decrease with the increase in flow rate, as shown in Fig. 1(c). In

addition, the estimated t_m for chlorobenzene (Table S4†) is much smaller than its measured tubing delay. By contrast, the estimated t_m for isoprene (Table S3†) is comparable to its measured tubing delays at different flow rates. These results indicate that gas–surface interactions play predominant roles in determining the tubing delays of organic compounds, particularly for the species with smaller C^* values associated with tubing delays much larger than several seconds. The effects of molecular diffusion and dispersion become more important for the species with larger C^* values associated with tubing delay in the range of several seconds.

Fig. 2 shows tubing delays of organic compounds as a function of C^*, residence time, tubing length, and flow rate. Tubing delays of organic compounds with different tubing lengths and flow rates all exhibit exponential decreases with the increase in C^*, as shown in Fig. 2(a). This is consistent with the work
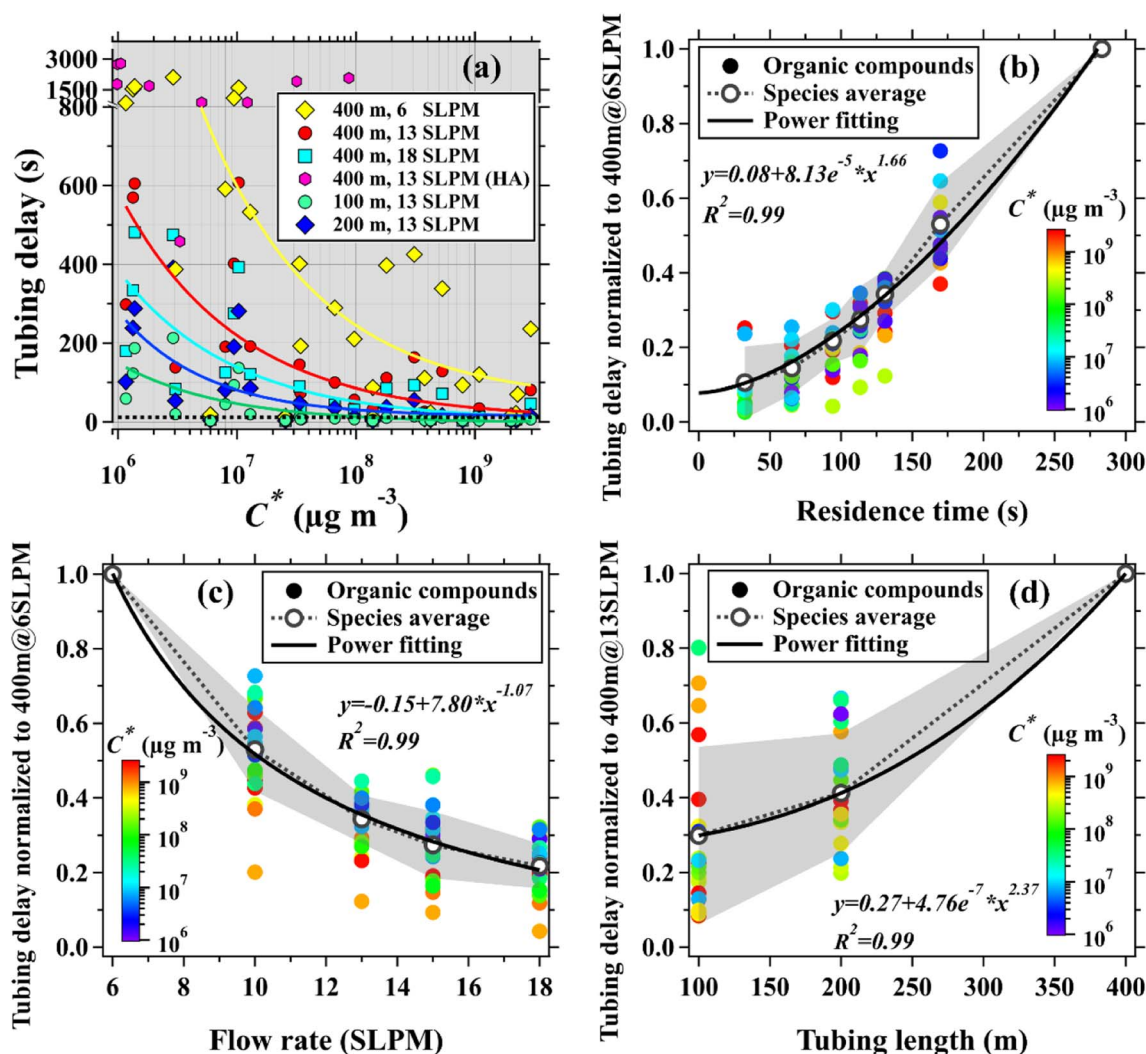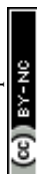

Fig. 2 Tubing delays of various organic compounds as a function of (a) C^*, (b) residence time, (c) tubing length, and (d) flow rate; In panel (a), HA is the abbreviation for higher alkanes that were measured by PTR-ToF-MS in NO$^+$ mode; the solid lines indicate power fittings; the black dashed line indicates the potential maximum t_m for an organic compound with large molecular weight after traversing the 400 m long tubing at a flow rate of 13 SLPM. In panels (b and c), tubing delays of organic compounds were normalized to those measured for the 400 m long tubing at a flow rate of 6 SLPM. In panel (d), tubing delays were normalized to those measured for the 400 m long tubing at a flow rate of 13 SLPM. In panels (b–d), circles are color coded by C^*.

reported in ref. 44. Tubing delays of the organic compounds with small C^* values (*e.g.*, $C^* < 5.0 \times 10^6$ µg m^{-3}) are much higher than those of the species with large C^* values. In addition to higher alkanes (HA), tubing delays of the majority of the organic compounds with C^* greater than 5.0×10^6 µg m^{-3} in the 400 m long tubing are lower than 200 s at the flow rate of 13 SLPM. For organic compounds with C^* between 1.0×10^6 and 5.0×10^6 µg m^{-3}, their tubing delays are generally lower than 600 s. As a result, the time scales for averaging concentrations of these organic compounds should be greater than their tubing delays. For example, 10 min (or more) mean concentrations of the organic compounds with C^* between 1.0×10^6 and 5.0×10^6 µg m^{-3} made by the 400 m long tubing at the flow rate of 13 SLPM are more reliable for subsequent analysis.

As discussed above, the tubing delay of an organic compound is closely associated with the residence time of the air sample stream in the tubing. As shown in Fig. 2(b), tubing delays of organic compounds increase rapidly with the increase in residence time. The residence time of the air sample stream in a tubing is mainly determined by the tubing length and flow rate. Therefore, we further investigate responses of tubing delays of targeted organic compounds to changes in tubing length and flow rate in this study, as shown in Fig. 2(c) and (d).

Tubing delays of organic compounds increase rapidly with the decrease in flow rate. The increase in the flow rate of the air sample stream can also enhance the molecular diffusion/dispersion of trace gases in the radial direction of the tubing,[45] leading to a decline in the time required for achieving the absorption–desorption equilibriums of various trace gases. Under these conditions, the flow rate of the air sample stream in long tubing should be as large as possible if instrument configurations are allowed. For a fixed flow rate of 13 SLPM, tubing delays of organic compounds also increase rapidly with the increase in tubing length. However, the tubing delays of organic compounds exhibit slight non-linear responses to changes in both tubing length and flow rate. These results are slightly different from those reported by the previous work[44] that delay times of organic compounds are proportional to tubing length and are inversely proportional to flow rate. Previous work[44] mainly focused on tubing delays of the organic compounds that have small C^* values in tubes with short lengths (<3 m), small ODs (≤1/4″) and flow rates (≤3 SLPM, laminar flow). Reynolds numbers of sample gas streams in the tubing (OD: 1/2″) used in this study are generally larger (∼900–2700) than those used in the literature (≤1000).[40,41,44] Therefore, the air sample streams in long tubes in this study are close to
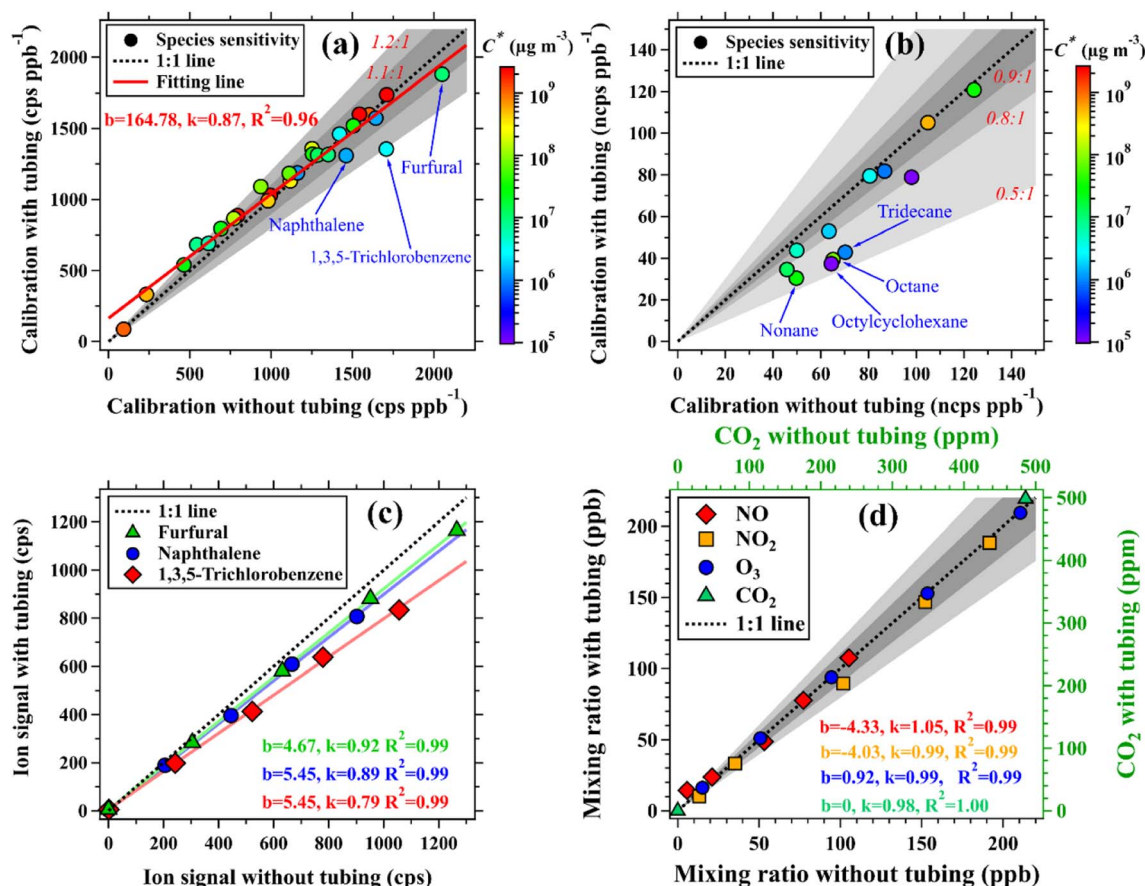

Fig. 3 Intercomparison of species signals/mixing ratios measured with and without the 400 m long tubing at a flow rate of 13 SLPM. (a and b) Calibration of the organic compounds measured by PTR-ToF-MS in H$_3$O and NO modes, respectively; markers are color coded by C^*. (c) Ion signals of three typical organic compounds with large tubing delays measured by PTR-ToF-MS in H$_3$O mode. (d) Mixing ratios of NO, NO$_2$, O$_3$, and CO$_2$. Solid lines in panels (a) and (c) are linear fittings ($y = kx + b$).

© 2023 The Author(s). Published by the Royal Society of Chemistry

Environ. Sci.: Atmos., 2023, **3**, 506–520 | **511**

the transition between the laminar and turbulent flow. In addition, the increase in tubing length and flow rate will non-linearly enhance the impacts from molecular diffusion and dispersion on measured concentrations of trace gases after traversing the tubing. These are the two most likely reasons for the slight non-linear responses of tubing delays of organic compounds to changes in tubing length and flow rate.

3.2. Interactions between tubing and various trace gases

In this study, the impacts of long tubing on changes in measured concentrations of targeted trace gases were mainly assessed using a 400 m long tube, as detailed in the ESI.† The assessment was first performed in the laboratory by measuring known concentrations of targeted trace gases with and without the tubing. The duration time of each concentration step is ~30 min for PTR-ToF-MS in H_3O^+ mode and ~50 min for PTR-ToF-MS in NO^+ mode (Fig. S4†). For the organic compounds that have tubing delays smaller than the time between concentration steps, their ion signals measured at both ends of the tubing agreed well within 20%, as shown in Fig. 3. By contrast, ion signals of the organic compounds measured at the two ends of the tubing will significantly deviate if their tubing delays are larger or comparable to the time between concentration steps. For example, ion signals of the species with small C^* values, namely naphthalene, 1,3,5-trichlorobenzene, tridecane, octane, octylcyclohexane, and nonane, measured with the tubing were 11–50% lower than those measured without the tubing. As introduced in Section 2.2, the tubing delay of a trace gas is defined as the amount of time required to reach 90% of the total change in its concentration and thus more time will be required for the last 10% of the change (Fig. S9 and S10†). However, concentrations of an organic compound measured with and without the tubing do not have detectable differences when its tubing delay is much smaller than the time between concentration steps. In contrast to organic compounds, concentrations of NO, NO_2, O_3, and CO_2 measured at both ends of the 400 m long tubing agreed well within 5%, as shown in Fig. 3(d).

Measurement uncertainties of various organic compounds in the 400 m long tubing (two 200 m long tubes at 120 m height of the SMT) during the field campaign were also assessed by adding the mixture of gas standards and zero air to the inlet end at the ground. As shown in Fig. S15,† ion signals measured with and without the 400 m long tubing also agreed well ($k = 0.85$, $R^2 = 0.88$). These results further confirm the effectiveness of the observations made by the vertical observation system developed in this study.

In addition to the impacts from tubing delays, many trace gases may be chemically consumed/formed to varying degrees when traversing the tubing. The tubes were mounted in dark environments to prevent photochemical reactions of reactive trace gases. Chemical reactions had minor impacts on measurements of trace gases made in the nighttime due to the absence of sunlight outside. By contrast, this is highly important for measurements of reactive species in the daytime when they are drawn into the tubing (the absence of sunlight) from
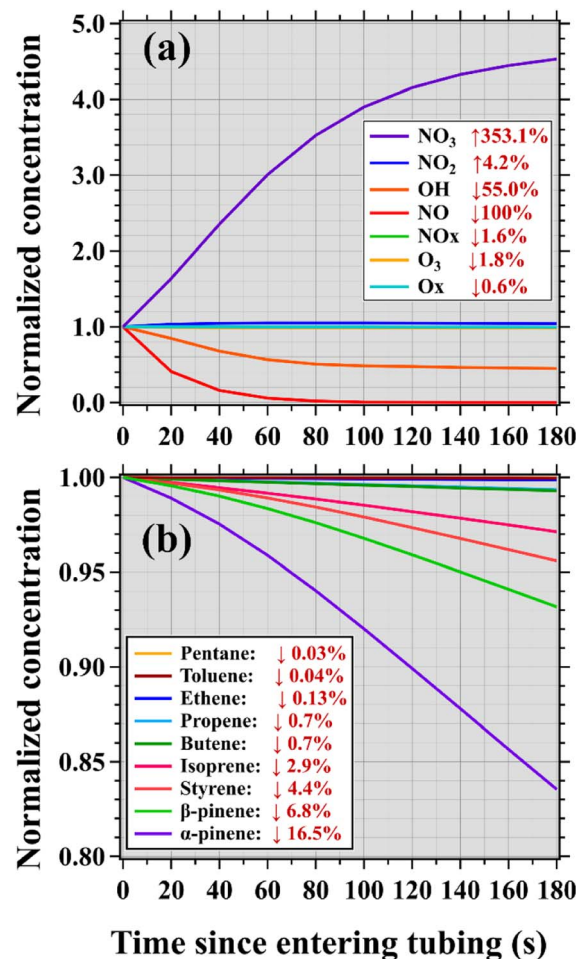

Fig. 4 Time series of concentrations of various chemical species since setting solar irradiation as zero (entering the tubing, $t = 0$) in the box model when the initial mixing ratio of ozone was set as 100 ppb. Concentrations of the chemical species were normalized to those at $t = 0$ s.

ambient air (the presence of sunlight). According to the box model results (Fig. 4), concentrations of the hydroxyl radical (OH) decrease by 55% while concentrations of the nitrate radical (NO_3) increase by more than a factor of 3 in the following 180 s (Fig. S14†) after setting solar radiation to zero (entering the tubing) when the ambient ozone mixing ratio was 100 ppb. NO will be completely consumed in less than 100 s, accompanied by an increase of 4.2% in NO_2 and a decrease of 1.8% in ozone. As a result, accurate measurements of NOx and Ox can be made by using long PFA Teflon tubes in both the daytime and nighttime, while concentrations of ozone and NO can be well measured only at night.

In the absence of sunlight, the primary degradation pathways of hydrocarbons (e.g., NO_3- and ozone-initiated reactions) are quite different from those in the daytime due to the rapid decline in concentrations of OH radicals. Therefore, the loss amount of an organic compound after traversing long tubing is mainly dependent on its reaction rate constant to the NO_3 radical (k_{NO_3}). As indicated in the literature,[55,56] k_{NO_3} values for

512 | Environ. Sci.: Atmos., 2023, **3**, 506–520

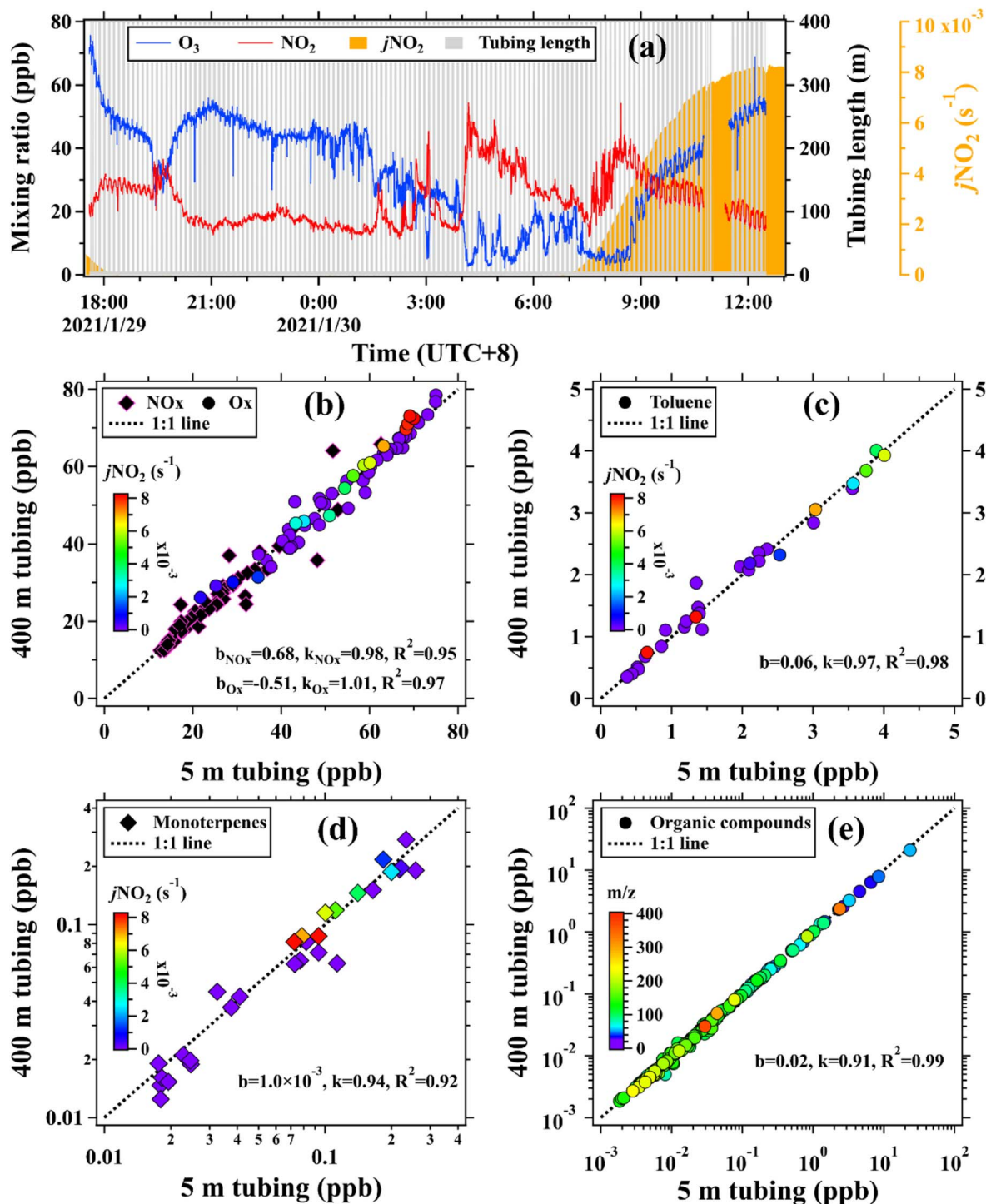© 2023 The Author(s). Published by the Royal Society of Chemistry

Fig. 5   (a) Time series of ozone and NO_2 mixing ratios along with the photolysis rate of NO_2, denoted by jNO_2, measured at ground level at the SMT site. (b–d) Intercomparisons of species mixing ratios that were averaged in time intervals of 10 min. (e) Intercomparison of mixing ratios of various organic compounds that were averaged over the whole measurement period.

most alkenes, particularly for monoterpenes, are greater than those for alkanes, aromatics, and oxygenated VOCs. Therefore, the decrease in concentrations of α-pinene (16.5%, $k_{NO_3} = 6.16 \times 10^{-12}$ cm^3 molec.$^{-1}$ s^{-1} at 298 K here and afterwards) is the most significant in the following 180 s after entering the tubing, followed by β-pinene (4.15%, $k_{NO_3} = 2.51 \times 10^{-12}$ cm^3 molec.$^{-1}$

s^{-1}), styrene (4.4%, $k_{NO_3} = 1.5 \times 10^{-12}$ cm^3 molec.$^{-1}$ s^{-1}), and isoprene (2.9%, $k_{NO_3} = 7.0 \times 10^{-13}$ cm^3 molec.$^{-1}$ s^{-1}). As for other alkene and alkane species with smaller k_{NO_3} values (<10^{-14} cm^3 molec.$^{-1}$ s^{-1}) and were predominantly emitted by anthropogenic sources, negligible decreases in their concentrations (<1%) were estimated. As shown in Fig. S16,† smaller decreases

in concentrations of these reactive VOCs were estimated after traversing the tubing when ambient ozone was only 50 ppb in comparison to those calculated for ambient ozone of 100 ppb (Fig. 4).

To further assess the impacts of long tubing on measurements of trace gases in real environments, ambient concentrations of O_3, NO_x, and a large set of organic compounds were alternatively measured by using a 5 m and a 400 m long tubing, as shown in Fig. 5. Concentrations of Ox ($k = 1.01$, $R^2 = 0.97$) and NO_x ($k = 0.98$, $R^2 = 0.95$) measured by using the two tubes agreed well within 2%. As expected, concentrations of O_3 and NO measured using the two tubes agreed well at nighttime. By contrast, concentrations of O_3 and NO measured using the 400 m long tubing in daylight (LT 07:00–13:00) decreased on average by 18% and 53%, respectively, in comparison to those made using the 5 m long tubing (Fig. S17†).

For organic compounds with low NO_3 reactivities, taking toluene as an example, their concentrations agreed quite well when measured using the two tubes with different lengths. The most concerned organic compounds are monoterpenes due to their large NO_3 reactivities and notable potential losses after traversing the 400 m long tubing in the daytime. However, insignificant discrepancies in concentrations of monoterpenes measured using the two tubes were observed in both the daytime and nighttime, as shown in Fig. 5(d). The maximum ozone concentration at ground level before LT 13:00 on January 30, 2021 was only 55.1 ppb, resulting in lower mixing ratios of NO_3 radicals and smaller losses of reactive monoterpene species in the tubing (Fig. S16†) than those when ambient ozone concentration was 100 ppb (Fig. 4). It should be noted that the box model results only estimated the potential maximum changes in concentrations of the targeted species after traversing the tubing. In real environments, the situation is much more complicated than the settings of model simulations. The expected changes in concentrations of the targeted trace gases may be lower than those predicted by the model results. In addition, ambient concentrations of monoterpenes were relatively low (~0.1 ppb) in the daytime and changed over time. As a result, the small losses of monoterpenes concentrations (only several ppt) after traversing the tubing cannot be well identified by comparisons of their ambient measurements.

In addition to the organic compounds contained in the gas standard, we also compared the mean mixing ratios of 207 species measured by PTR-ToF-MS using the two different tubes. Concentrations of these species were calculated using the method based on the reaction kinetics of the PTR-ToF-MS, as detailed in our previous studies.[46,47,57] As shown in Fig. 5(e), the mixing ratios of the selected species, averaged over the whole period, agreed well ($k = 0.91$, $R^2 = 0.99$) when measured using the 5 m and the 400 m long tubes.

Lastly, an intercomparison of ozone, Ox, NO, and NO_x measurements made by the vertical observation system (observations by tubing) and different tower platforms (*in situ* observations) was conducted from January 8 to 26, 2021. As shown in Fig. 6(a) and (b), mixing ratios of NO_x ($k = 0.89$, $R^2 = 0.92$) and Ox ($k = 0.97$, $R^2 = 0.92$) measured by the vertical

observation system agreed well with *in situ* observations. Owing to the absence of sunlight in both the tubing and ambient air at night, reliable measurements of ozone and NO could be made by the vertical observation system (low ozone but high NO concentrations, as shown in Fig. 6, S18 and S19†). In contrast to NO, we also believe that the ozone measurements made by long tubes in the daytime can be used to characterize its vertical distributions (Fig. S19†) due to the fact that NO concentrations in the daytime (high ozone concentrations) were generally very low and decreased with height (Fig. S20†). For example, the mean NO mixing ratio at 335 m between LT 11:00 and 16:00 over the period of January 8 to 25, 2021 was only 5.3 ± 3.5 ppb, which was much lower than that of ozone (53.1 ± 18.5 ppb). Therefore, the amount of ozone consumed by NO in the daytime when traversing the tubing was very limited. In addition, we also compared the mean vertical profiles of NO_x and Ox mixing ratios made by the two approaches in the nighttime (LT 0:00–06:00) from January 13 to 15, 2021, as shown in Fig. 6(e) and (f). The nighttime data were used due to the fact that the vertical gradients of NO_x and Ox mixing ratios were more pronounced in the nighttime than in the daytime (Fig. S21†). The vertical profiles of NO_x ($r = 0.99$) and Ox ($r = 0.67$) made by the two approaches are also well correlated.

3.3. Vertical observations of atmospheric trace gases

A field campaign was conducted at the SMT in January 2021 to make vertical gradient measurements of trace gases using the vertical observation system established in this study. Fig. 7 shows the time series of mixing ratios of five selected species, namely NO_x, Ox, CO_2, toluene, and acetone, during LT 0:00–1:00 on January 16 along with their vertical profiles averaged over the period of January 14 to 29, 2021. The vertical observation system can obtain stable measurements of these chemical species after the switch of the inlet heights and can also well characterize their vertical distributions.

Vertical profiles of NO_x, toluene, and acetone exhibited weak gradients in the daytime due to strong atmospheric vertical mixing, which was consistent with the results reported in the literature.[58–60] In the nighttime, mixing ratios of NO_x, toluene, and acetone below 120 m were markedly higher than those aloft, predominantly attributed to the combined effect of strong source emissions (*e.g.*, vehicular exhausts) and suppressed vertical mixing.[61,62] Ox is a conserved metric to characterize the spatio-temporal variability of ozone by removing the NO titration effect.[4,63] The positive gradients in Ox profiles in both the daytime and nighttime were predominantly caused by surface dry deposition and chemical removal.[64,65] Mixing ratios of CO_2 in daytime exhibited positive gradients below 120 m due to the photosynthetic consumption of vegetation. In the nighttime, CO_2 mixing ratios rapidly decreased from the surface to 120 m due to the combined effect of enhanced source emissions (*e.g.*, biological respiration and fossil fuel combustion) and suppressed vertical mixing. By contrast, CO_2 mixing ratios were well mixed above 120 m in both the daytime and nighttime owing to its stable chemical properties. In addition to the chemical species that have small tubing delays (Fig. 7), the vertical
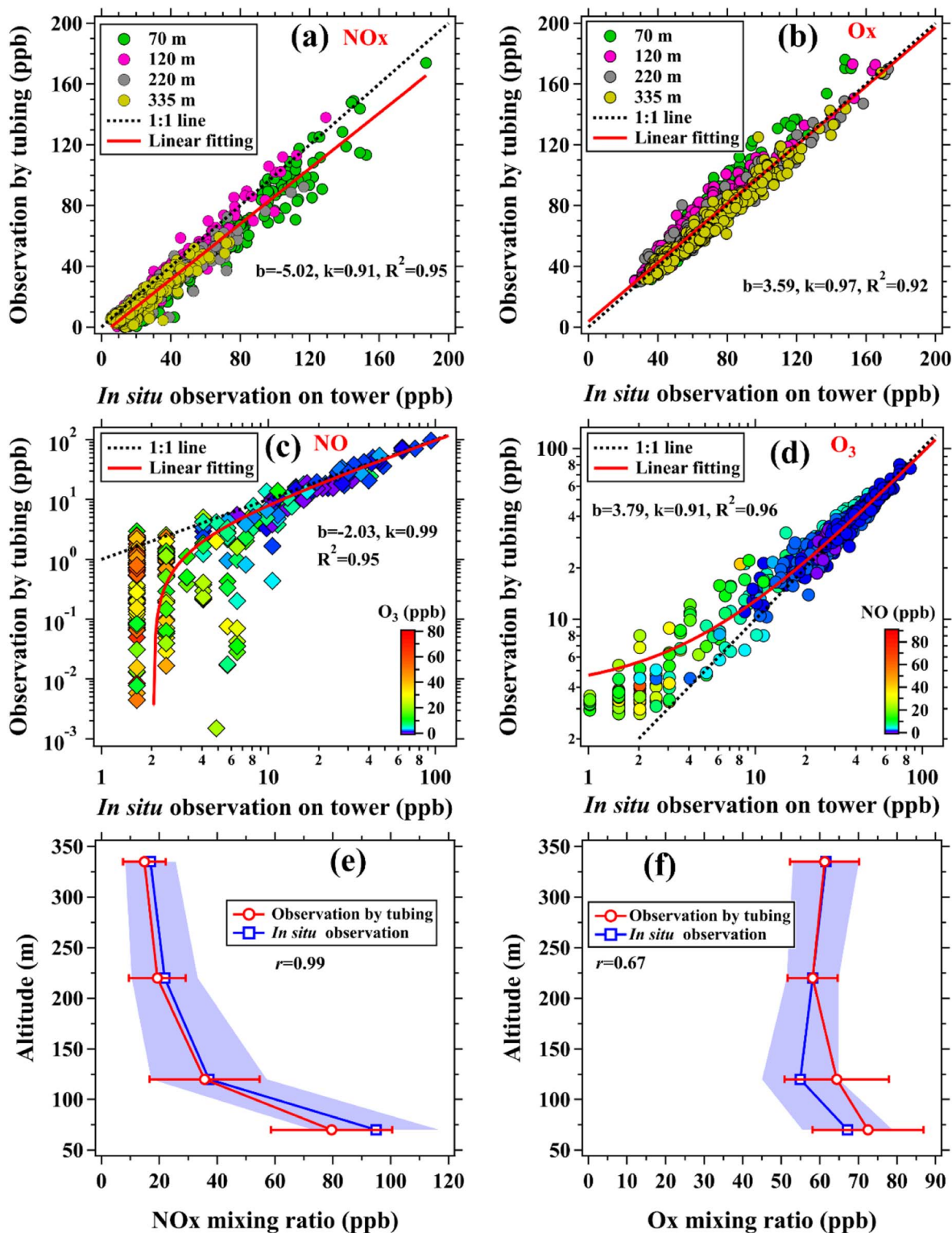
Fig. 6 (a–d) Intercomparisons of NOx, Ox, NO, and O_3 mixing ratios (hourly averages) measured by the vertical observation system (long tubing) and tower platforms (*in situ* observations) from January 8 to January 26, 2021; Solid lines are linear fittings ($y = kx + b$). (e and f) Intercomparison of mean vertical profiles of NOx and Ox mixing ratios in the nighttime (LT 0:00–06:00) from January 13 to 15, 2021; *r* is Pearson's correlation coefficient.

observation system can also well capture vertical variations in concentrations of the organic compounds with small *C** values (*e.g.*, phenol, furfural, guaiacol, and naphthalene), as shown in

Fig. S22.† More results and analysis about the gradient measurements of the trace gases will be presented and discussed in our future studies.

© 2023 The Author(s). Published by the Royal Society of Chemistry

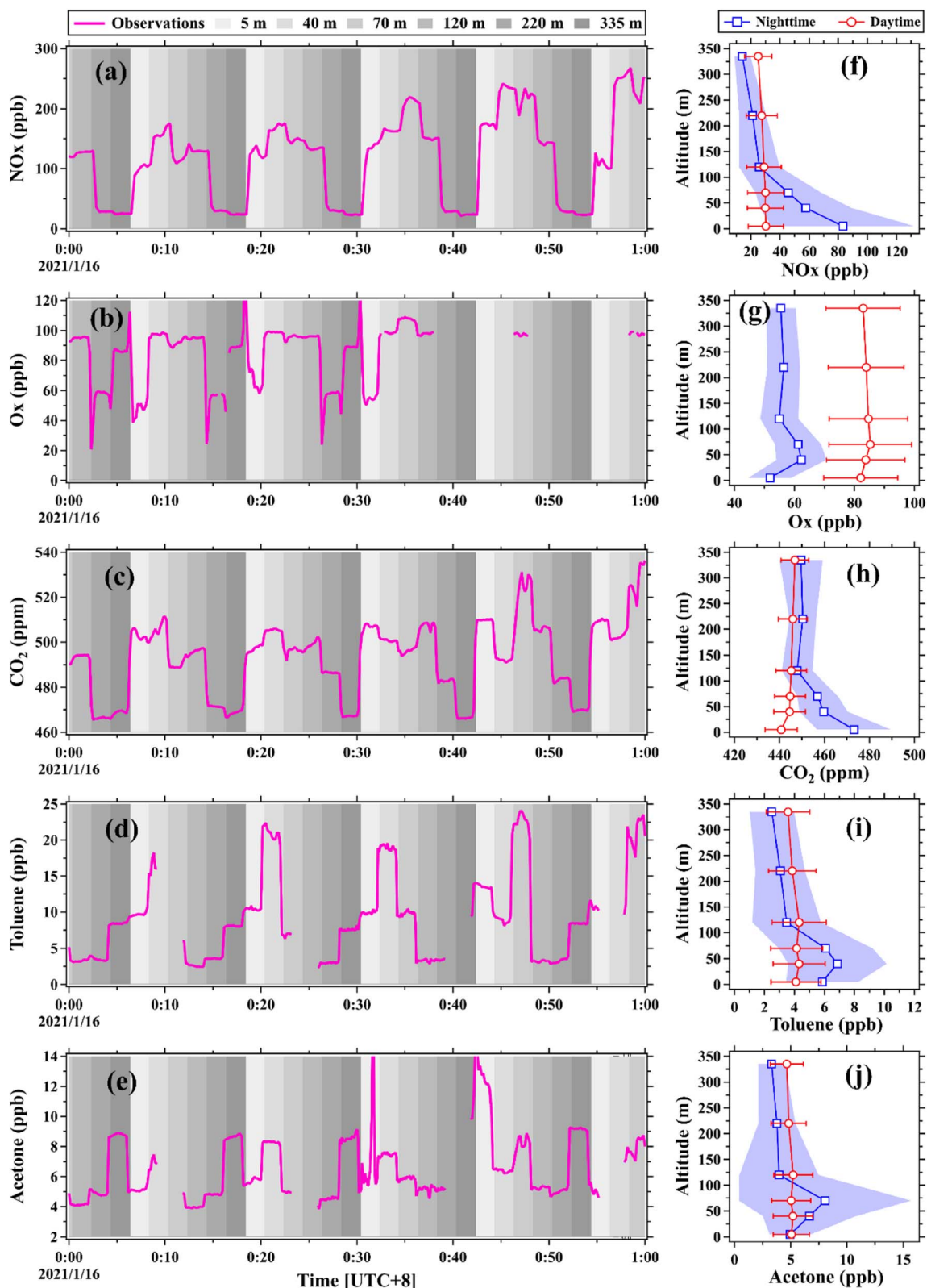*Environ. Sci.: Atmos.*, 2023, **3**, 506–520 | **515**

Fig. 7 (a–e) Time series of mixing ratios of the selected chemical species measured by the vertical observation system at the SMT site. (f–j) Mean vertical profiles of the selected chemical species (mean ± 0.5 standard deviations) for the daytime (LT 10:00–16:00) and nighttime (LT 22:00–05:00) from January 16 to 29, 2021.

4. Conclusions

In summary, long PFA Teflon tubes performed well in sampling ambient air for analyzing concentrations and spatio-temporal variations of atmospheric trace gases. To reduce tubing delays of the organic compounds with small C^* values, PFA Teflon tubes with larger inner diameters and flow rates are recommended if instruments allow. Apart from NO in the daytime, insignificant losses were observed for concentrations of most of the atmospheric trace gases in both the daytime and nighttime. Field observations also confirmed that concentrations of many trace gases could be well measured by the vertical observation system developed in this study.

In addition to tall towers or high-rise buildings, PFA Teflon tubes can also be used to establish vertical observation systems of atmospheric trace gases based on mobile platforms, such as tethered balloons[15,43] and UAVs. In addition, a similar method using PFA Teflon tubes can be developed to surveil emissions of targeted chemical species at multiple locations, such as distributed industrial parks.[66] The results of this study could provide a solid theoretical basis for the utilization of long PFA Teflon tubes in these applications and provide better guidance in the assessment of their data quality.

Author contributions

XBL and BY designed the research. XBL, CZ, AL, BY, CL, SW, YH, JQ, ZL, XH, XS, YC, XZ, EZ, LY, QY, GQ, and JZ contributed to the data collection and data analysis. XBL, BY, and YP performed the box model simulation analysis. XBL and BY wrote the paper with contributions from all coauthors. All the coauthors discussed the results and reviewed the paper.

Conflicts of interest

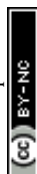There are no conflicts to declare.

Acknowledgements

References

1 C. Wu, B. Liu, D. Wu, H. Yang, X. Mao, J. Tan, Y. Liang, J. Y. Sun, R. Xia, J. Sun, G. He, M. Li, T. Deng, Z. Zhou and Y. J. Li, Vertical profiling of black carbon and ozone using a multicopter unmanned aerial vehicle (UAV) in urban Shenzhen of South China, *Sci. Total Environ.*, 2021, **801**, 149689.

2 K. Zhang, L. Zhou, Q. Fu, L. Yan, Q. Bian, D. Wang and G. Xiu, Vertical distribution of ozone over Shanghai during late spring: A balloon-borne observation, *Atmos. Environ.*, 2019, **208**, 48–60.

3 V. Ramanathan and Y. Feng, Air pollution, greenhouse gases and climate change: Global and regional perspectives, *Atmos. Environ.*, 2009, **43**, 37–50.

4 X.-B. Li, B. Yuan, D. D. Parrish, D. Chen, Y. Song, S. Yang, Z. Liu and M. Shao, Long-term trend of ozone in southern China reveals future mitigation strategy for air pollution, *Atmos. Environ.*, 2022, **269**, 118869.

5 M. S. Uddin and O. Smirnov, Spatial Distribution of the Annual Atmospheric Carbon Dioxide in the Contiguous USA and Their Controlling Factors, *Environ. Model. Assess.*, 2022, **27**, 57–76.

6 K. Li, D. J. Jacob, H. Liao, L. Shen, Q. Zhang and K. H. Bates, Anthropogenic drivers of 2013–2017 trends in summer surface ozone in China, *Proc. Natl. Acad. Sci. U. S. A.*, 2019, **116**, 422–427.

7 Z. Mo, S. Huang, B. Yuan, C. Pei, Q. Song, J. Qi, M. Wang, B. Wang, C. Wang, M. Li, Q. Zhang and M. Shao, Deriving emission fluxes of volatile organic compounds from tower observation in the Pearl River Delta, China, *Sci. Total Environ.*, 2020, **741**, 139763.

8 K. Glaser, U. Vogt, G. Baumbach, A. Volz-Thomas and H. Geiss, Vertical profiles of O_3, NO_2, NOx, VOC, and meteorological parameters during the Berlin Ozone Experiment (BERLIOZ) campaign, *J. Geophys. Res.: Atmos.*, 2003, **108**(D4), 8253.

9 G. Sangiorgi, L. Ferrero, M. G. Perrone, E. Bolzacchini, M. Duane and B. R. Larsen, Vertical distribution of hydrocarbons in the low troposphere below and above the mixing height: Tethered balloon measurements in Milan, Italy, *Environ. Pollut.*, 2011, **159**, 3545–3552.

10 E. Velasco, C. Marquez, E. Bueno, R. M. Bernabe, A. Sanchez, O. Fentanes, H. Wohrnschimmel, B. Cardenas, A. Kamilla, S. Wakamatsu and L. T. Molina, Vertical distribution of ozone and VOCs in the low boundary layer of Mexico City, *Atmos. Chem. Phys.*, 2008, **8**, 3061–3079.

11 J. Li, Q. Fu, J. Huo, D. Wang, W. Yang, Q. Bian, Y. Duan, Y. Zhang, J. Pan, Y. Lin, K. Huang, Z. Bai, S.-H. Wang, J. S. Fu and P. K. K. Louie, Tethered balloon-based black carbon profiles within the lower troposphere of Shanghai in the 2013 East China smog, *Atmos. Environ.*, 2015, **123**, 327–338.

12 S. J. Oltmans, B. J. Johnson, J. M. Harris, A. M. Thompson, H. Y. Liu, C. Y. Chan, H. Vömel, T. Fujimoto, V. G. Brackett, W. L. Chang, J.-P. Chen, J. H. Kim, L. Y. Chan and H.-W. Chang, Tropospheric ozone over the North Pacific from ozonesonde observations, *J. Geophys. Res.: Atmos.*, 2004, **109**, D15S01.

13 D. Helmig, B. Johnson, S. J. Oltmans, W. Neff, F. Eisele and D. D. Davis, Elevated ozone in the boundary layer at South Pole, *Atmos. Environ.*, 2008, **42**, 2788–2803.

14 D. Helmig, B. J. Johnson, M. Warshawsky, T. Morse, W. D. Neff, F. Eisele and D. D. Davis, Nitric oxide in the boundary-layer at South Pole during the Antarctic Tropospheric Chemistry Investigation (ANTCI), *Atmos. Environ.*, 2008, **42**, 2817–2830.

© 2023 The Author(s). Published by the Royal Society of Chemistry

Environ. Sci.: Atmos., 2023, **3**, 506–520 | 517

15 B. J. Johnson, D. Helmig and S. J. Oltmans, Evaluation of ozone measurements from a tethered balloon-sampling platform at South Pole Station in December 2003, *Atmos. Environ.*, 2008, **42**, 2780–2787.

16 T.-D.-H. Vo, C. Lin, C.-E. Weng, C.-S. Yuan, C.-W. Lee, C.-H. Hung, X.-T. Bui, K.-C. Lo and J.-X. Lin, Vertical stratification of volatile organic compounds and their photochemical product formation potential in an industrial urban area, *J. Environ. Manage.*, 2018, **217**, 327–336.

17 C.-C. Chang, J.-L. Wang, C.-Y. Chang, M.-C. Liang and M.-R. Lin, Development of a multicopter-carried whole air sampling apparatus and its applications in environmental studies, *Chemosphere*, 2016, **144**, 484–492.

18 V. Lambey and A. D. Prasad, A Review on Air Quality Measurement Using an Unmanned Aerial Vehicle, *Water, Air, Soil Pollut.*, 2021, **232**, 109.

19 Z. Mo, S. Huang, B. Yuan, C. Pei, Q. Song, J. Qi, M. Wang, B. Wang, C. Wang and M. Shao, Tower-based measurements of NMHCs and OVOCs in the Pearl River Delta: Vertical distribution, source analysis and chemical reactivity, *Environ. Pollut.*, 2022, **292**, 118454.

20 H. Zhang, Y. Zhang, Z. Huang, W. J. F. Acton, Z. Wang, E. Nemitz, B. Langford, N. Mullinger, B. Davison, Z. Shi, D. Liu, W. Song, W. Yang, J. Zeng, Z. Wu, P. Fu, Q. Zhang and X. Wang, Vertical profiles of biogenic volatile organic compounds as observed online at a tower in Beijing, *J. Environ. Sci.*, 2020, **95**, 33–42.

21 A. K. Benton, J. M. Langridge, S. M. Ball, W. J. Bloss, M. Dall'Osto, E. Nemitz, R. M. Harrison and R. L. Jones, Night-time chemistry above London: measurements of NO_3 and N_2O_5 from the BT Tower, *Atmos. Chem. Phys.*, 2010, **10**, 9781–9795.

22 S. S. Brown, H. An, M. Lee, J.-H. Park, S.-D. Lee, D. L. Fibiger, E. E. McDuffie, W. P. Dubé, N. L. Wagner and K.-E. Min, Cavity enhanced spectroscopy for measurement of nitrogen oxides in the Anthropocene: results from the Seoul tower during MAPS 2015, *Faraday Discuss.*, 2017, **200**, 529–557.

23 M. O. Andreae, O. C. Acevedo, A. Araùjo, P. Artaxo, C. G. G. Barbosa, H. M. J. Barbosa, J. Brito, S. Carbone, X. Chi, B. B. L. Cintra, N. F. da Silva, N. L. Dias, C. Q. Dias-Júnior, F. Ditas, R. Ditz, A. F. L. Godoi, R. H. M. Godoi, M. Heimann, T. Hoffmann, J. Kesselmeier, T. Könemann, M. L. Krüger, J. V. Lavric, A. O. Manzi, A. P. Lopes, D. L. Martins, E. F. Mikhailov, D. Moran-Zuloaga, B. W. Nelson, A. C. Nölscher, D. Santos Nogueira, M. T. F. Piedade, C. Pöhlker, U. Pöschl, C. A. Quesada, L. V. Rizzo, C. U. Ro, N. Ruckteschler, L. D. A. Sá, M. de Oliveira Sá, C. B. Sales, R. M. N. dos Santos, J. Saturno, J. Schöngart, M. Sörgel, C. M. de Souza, R. A. F. de Souza, H. Su, N. Targhetta, J. Tóta, I. Trebs, S. Trumbore, A. van Eijck, D. Walter, Z. Wang, B. Weber, J. Williams, J. Winderlich, F. Wittmann, S. Wolff and A. M. Yáñez-Serrano, The Amazon Tall Tower Observatory (ATTO): overview of pilot measurements on ecosystem ecology, meteorology, trace gases, and aerosols, *Atmos. Chem. Phys.*, 2015, **15**, 10723–10776.

24 S. S. Brown, J. A. Thornton, W. C. Keene, A. A. P. Pszenny, B. C. Sive, W. P. Dubé, N. L. Wagner, C. J. Young, T. P. Riedel, J. M. Roberts, T. C. VandenBoer, R. Bahreini, F. Öztürk, A. M. Middlebrook, S. Kim, G. Hübler and D. E. Wolfe, Nitrogen, Aerosol Composition, and Halogens on a Tall Tower (NACHTT): Overview of a wintertime air chemistry field study in the front range urban corridor of Colorado, *J. Geophys. Res.: Atmos.*, 2013, **118**, 8067–8085.

25 X.-B. Li, G. Fan, S. Lou, B. Yuan, X. Wang and M. Shao, Transport and boundary layer interaction contribution to extremely high surface ozone levels in eastern China, *Environ. Pollut.*, 2021, **268**, 115804.

26 C. Xing, C. Liu, S. Wang, K. L. Chan, Y. Gao, X. Huang, W. Su, C. Zhang, Y. Dong, G. Fan, T. Zhang, Z. Chen, Q. Hu, H. Su, Z. Xie and J. Liu, Observations of the vertical distributions of summertime atmospheric pollutants and the corresponding ozone production in Shanghai, China, *Atmos. Chem. Phys.*, 2017, **17**, 14275–14289.

27 Q. Hong, L. Zhu, C. Xing, Q. Hu, H. Lin, C. Zhang, C. Zhao, T. Liu, W. Su and C. Liu, Inferring vertical variability and diurnal evolution of O_3 formation sensitivity based on the vertical distribution of summertime HCHO and NO_2 in Guangzhou, China, *Sci. Total Environ.*, 2022, **827**, 154045.

28 S. E. Benish, H. He, X. Ren, S. J. Roberts, R. J. Salawitch, Z. Li, F. Wang, Y. Wang, F. Zhang, M. Shao, S. Lu and R. R. Dickerson, Measurement report: Aircraft observations of ozone, nitrogen oxides, and volatile organic compounds over Hebei Province, China, *Atmos. Chem. Phys.*, 2020, **20**, 14523–14545.

29 S. S. Brown, W. P. Dubé, R. Bahreini, A. M. Middlebrook, C. A. Brock, C. Warneke, J. A. de Gouw, R. A. Washenfelder, E. Atlas, J. Peischl, T. B. Ryerson, J. S. Holloway, J. P. Schwarz, R. Spackman, M. Trainer, D. D. Parrish, F. C. Fehshenfeld and A. R. Ravishankara, Biogenic VOC oxidation and organic aerosol formation in an urban nocturnal boundary layer: aircraft vertical profiles in Houston, TX, *Atmos. Chem. Phys.*, 2013, **13**, 11317–11337.

30 X. Chen, D. B. Millet, H. B. Singh, A. Wisthaler, E. C. Apel, E. L. Atlas, D. R. Blake, I. Bourgeois, S. S. Brown, J. D. Crounse, J. A. de Gouw, F. M. Flocke, A. Fried, B. G. Heikes, R. S. Hornbrook, T. Mikoviny, K. E. Min, M. Müller, J. A. Neuman, D. W. O'Sullivan, J. Peischl, G. G. Pfister, D. Richter, J. M. Roberts, T. B. Ryerson, S. R. Shertz, C. R. Thompson, V. Treadaway, P. R. Veres, J. Walega, C. Warneke, R. A. Washenfelder, P. Weibring and B. Yuan, On the sources and sinks of atmospheric VOCs: an integrated analysis of recent aircraft campaigns over North America, *Atmos. Chem. Phys.*, 2019, **19**, 9097–9123.

31 B. Yuan, A. Koss, C. Warneke, J. B. Gilman, B. M. Lerner, H. Stark and J. A. de Gouw, A high-resolution time-of-flight chemical ionization mass spectrometer utilizing hydronium ions (H_3O^+ ToF-CIMS) for measurements of

volatile organic compounds in the atmosphere, *Atmos. Meas. Tech.*, 2016, **9**, 2735–2752.

32 J. A. Fisher, D. J. Jacob, K. R. Travis, P. S. Kim, E. A. Marais, C. C. Miller, K. Yu, L. Zhu, R. M. Yantosca, M. P. Sulprizio, J. Mao, P. O. Wennberg, J. D. Crounse, A. P. Teng, T. B. Nguyen, J. M. St. Clair, R. C. Cohen, P. Romer, B. A. Nault, P. J. Wooldridge, J. L. Jimenez, P. Campuzano-Jost, D. A. Day, W. Hu, P. B. Shepson, F. Xiong, D. R. Blake, A. H. Goldstein, P. K. Misztal, T. F. Hanisco, G. M. Wolfe, T. B. Ryerson, A. Wisthaler and T. Mikoviny, Organic nitrate chemistry and its implications for nitrogen budgets in an isoprene- and monoterpene-rich atmosphere: constraints from aircraft (SEAC(4)RS) and ground-based (SOAS) observations in the Southeast US, *Atmos. Chem. Phys.*, 2016, **16**, 5969–5991.

33 V. T. Dieu Hien, C. Lin, V. C. Thanh, N. T. Kim Oanh, B. X. Thanh, C.-E. Weng, C.-S. Yuan and E. R. Rene, An overview of the development of vertical sampling technologies for ambient volatile organic compounds (VOCs), *J. Environ. Manage.*, 2019, **247**, 401–412.

34 X.-B. Li, D.-S. Wang, Q.-C. Lu, Z.-R. Peng and Z.-Y. Wang, Investigating vertical distribution patterns of lower tropospheric $PM_{2.5}$ using unmanned aerial vehicle measurements, *Atmos. Environ.*, 2018, **173**, 62–71.

35 L. Li, C. Lu, P.-W. Chan, X. Zhang, H.-L. Yang, Z.-J. Lan, W.-H. Zhang, Y.-W. Liu, L. Pan and L. Zhang, Tower observed vertical distribution of $PM_{2.5}$, O_3 and NO_x in the Pearl River Delta, *Atmos. Environ.*, 2020, **220**, 117083.

36 A. E. Andrews, J. D. Kofler, M. E. Trudeau, J. C. Williams, D. H. Neff, K. A. Masarie, D. Y. Chao, D. R. Kitzis, P. C. Novelli, C. L. Zhao, E. J. Dlugokencky, P. M. Lang, M. J. Crotwell, M. L. Fischer, M. J. Parker, J. T. Lee, D. D. Baumann, A. R. Desai, C. O. Stanier, S. F. J. De Wekker, D. E. Wolfe, J. W. Munger and P. P. Tans, CO_2, CO, and CH_4 measurements from tall towers in the NOAA Earth System Research Laboratory's Global Greenhouse Gas Reference Network: instrumentation, uncertainty analysis, and recommendations for future high-accuracy greenhouse gas monitoring efforts, *Atmos. Meas. Tech.*, 2014, **7**, 647–687.

37 L. Hu, D. B. Millet, M. J. Mohr, K. C. Wells, T. J. Griffis and D. Helmig, Sources and seasonality of atmospheric methanol based on tall tower measurements in the US Upper Midwest, *Atmos. Chem. Phys.*, 2011, **11**, 11145–11156.

38 F. A. Squires, E. Nemitz, B. Langford, O. Wild, W. S. Drysdale, W. J. F. Acton, P. Fu, C. S. B. Grimmond, J. F. Hamilton, C. N. Hewitt, M. Hollaway, S. Kotthaus, J. Lee, S. Metzger, N. Pingintha-Durden, M. Shaw, A. R. Vaughan, X. Wang, R. Wu, Q. Zhang and Y. Zhang, Measurements of traffic-dominated pollutant emissions in a Chinese megacity, *Atmos. Chem. Phys.*, 2020, **20**, 8737–8761.

39 W. J. F. Acton, Z. H. Huang, B. Davison, W. S. Drysdale, P. Q. Fu, M. Hollaway, B. Langford, J. Lee, Y. H. Liu, S. Metzger, N. Mullinger, E. Nemitz, C. E. Reeves, F. A. Squires, A. R. Vaughan, X. M. Wang, Z. Y. Wang, O. Wild, Q. Zhang, Y. L. Zhang and C. N. Hewitt, Surface-

atmosphere fluxes of volatile organic compounds in Beijing, *Atmos. Chem. Phys.*, 2020, **20**, 15101–15125.

40 B. L. Deming, D. Pagonis, X. Liu, D. A. Day, R. Talukdar, J. E. Krechmer, J. A. de Gouw, J. L. Jimenez and P. J. Ziemann, Measurements of delays of gas-phase compounds in a wide variety of tubing materials due to gas–wall interactions, *Atmos. Meas. Tech.*, 2019, **12**, 3453–3461.

41 X. Liu, B. Deming, D. Pagonis, D. A. Day, B. B. Palm, R. Talukdar, J. M. Roberts, P. R. Veres, J. E. Krechmer, J. A. Thornton, J. A. de Gouw, P. J. Ziemann and J. L. Jimenez, Effects of gas–wall interactions on measurements of semivolatile compounds and small polar molecules, *Atmos. Meas. Tech.*, 2019, **12**, 3137–3149.

42 J. de Gouw and C. Warneke, Measurements of volatile organic compounds in the earth's atmosphere using proton-transfer-reaction mass spectrometry, *Mass Spectrom. Rev.*, 2007, **26**, 223–257.

43 D. Helmig, C. R. Thompson, J. Evans, P. Boylan, J. Hueber and J. H. Park, Highly Elevated Atmospheric Levels of Volatile Organic Compounds in the Uintah Basin, Utah, *Environ. Sci. Technol.*, 2014, **48**, 4707–4715.

44 D. Pagonis, J. E. Krechmer, J. de Gouw, J. L. Jimenez and P. J. Ziemann, Effects of gas–wall partitioning in Teflon tubing and instrumentation on time-resolved measurements of gas-phase organic compounds, *Atmos. Meas. Tech.*, 2017, **10**, 4687–4696.

45 A. Karion, C. Sweeney, P. Tans and T. Newberger, AirCore: An Innovative Atmospheric Sampling System, *J. Atmos. Ocean Technol.*, 2010, **27**, 1839–1853.

46 C. Wu, C. Wang, S. Wang, W. Wang, B. Yuan, J. Qi, B. Wang, H. Wang, C. Wang, W. Song, X. Wang, W. Hu, S. Lou, C. Ye, Y. Peng, Z. Wang, Y. Huangfu, Y. Xie, M. Zhu, J. Zheng, X. Wang, B. Jiang, Z. Zhang and M. Shao, Measurement report: Important contributions of oxygenated compounds to emissions and chemistry of volatile organic compounds in urban air, *Atmos. Chem. Phys.*, 2020, **20**, 14769–14785.

47 X. He, B. Yuan, C. Wu, S. Wang, C. Wang, Y. Huangfu, J. Qi, N. Ma, W. Xu, M. Wang, W. Chen, H. Su, Y. Cheng and M. Shao, Volatile organic compounds in wintertime North China Plain: Insights from measurements of proton transfer reaction time-of-flight mass spectrometer (PTR-ToF-MS), *J. Environ. Sci.*, 2022, **114**, 98–114.

48 C. Wang, B. Yuan, C. Wu, S. Wang, J. Qi, B. Wang, Z. Wang, W. Hu, W. Chen, C. Ye, W. Wang, Y. Sun, C. Wang, S. Huang, W. Song, X. Wang, S. Yang, S. Zhang, W. Xu, N. Ma, Z. Zhang, B. Jiang, H. Su, Y. Cheng, X. Wang and M. Shao, Measurements of higher alkanes using NO+ chemical ionization in PTR-ToF-MS: important contributions of higher alkanes to secondary organic aerosols in China, *Atmos. Chem. Phys.*, 2020, **20**, 14123–14138.

49 A. Matsunaga and P. J. Ziemann, Gas-Wall Partitioning of Organic Compounds in a Teflon Film Chamber and Potential Effects on Reaction Product and Aerosol Yield Measurements, *Aerosol Sci. Technol.*, 2010, **44**, 881–892.

50 J. E. Krechmer, D. A. Day, P. J. Ziemann and J. L. Jimenez, Direct Measurements of Gas/Particle Partitioning and Mass

© 2023 The Author(s). Published by the Royal Society of Chemistry

Environ. Sci.: Atmos., 2023, **3**, 506–520 | **519**

Accommodation Coefficients in Environmental Chambers, *Environ. Sci. Technol.*, 2017, **51**, 11867–11875.

51 L. Li, C. Lu, P.-W. Chan, Z. Lan, W. Zhang, H. Yang and H. Wang, Impact of the COVID-19 on the vertical distributions of major pollutants from a tower in the Pearl River Delta, *Atmos. Environ.*, 2022, **276**, 119068.

52 X.-B. Li, B. Yuan, S. Wang, C. Wang, J. Lan, Z. Liu, Y. Song, X. He, Y. Huangfu, C. Pei, P. Cheng, S. Yang, J. Qi, C. Wu, S. Huang, Y. You, M. Chang, H. Zheng, W. Yang, X. Wang and M. Shao, Variations and sources of volatile organic compounds (VOCs) in urban region: insights from measurements on a tall tower, *Atmos. Chem. Phys.*, 2022, **22**, 10567–10587.

53 G. M. Wolfe, M. R. Marvin, S. J. Roberts, K. R. Travis and J. Liao, The Framework for 0-D Atmospheric Modeling (F0AM) v3.1, *Geosci. Model Dev.*, 2016, **9**, 3309–3319.

54 S. Yang, B. Yuan, Y. Peng, S. Huang, W. Chen, W. Hu, C. Pei, J. Zhou, D. D. Parrish, W. Wang, X. He, C. Cheng, X. B. Li, X. Yang, Y. Song, H. Wang, J. Qi, B. Wang, C. Wang, C. Wang, Z. Wang, T. Li, E. Zheng, S. Wang, C. Wu, M. Cai, C. Ye, W. Song, P. Cheng, D. Chen, X. Wang, Z. Zhang, X. Wang, J. Zheng and M. Shao, The formation and mitigation of nitrate pollution: comparison between urban and suburban environments, *Atmos. Chem. Phys.*, 2022, **22**, 4539–4556.

55 R. Atkinson, D. L. Baulch, R. A. Cox, J. N. Crowley, R. F. Hampson, R. G. Hynes, M. E. Jenkin, M. J. Rossi, J. Troe and I. Subcommittee, Evaluated kinetic and photochemical data for atmospheric chemistry: Volume II – gas phase reactions of organic species, *Atmos. Chem. Phys.*, 2006, **6**, 3625–4055.

56 R. Atkinson and J. Arey, Atmospheric Degradation of Volatile Organic Compounds, *Chem. Rev.*, 2003, **103**, 4605–4638.

57 B. Yuan, A. R. Koss, C. Warneke, M. Coggon, K. Sekimoto and J. A. de Gouw, Proton-Transfer-Reaction Mass Spectrometry: Applications in Atmospheric Sciences, *Chem. Rev.*, 2017, **117**, 13187–13229.

58 X.-B. Li, Z.-R. Peng, D. Wang, B. Li, Y. Huangfu, G. Fan, H. Wang and S. Lou, Vertical distributions of boundary-layer ozone and fine aerosol particles during the emission control period of the G20 summit in Shanghai, China, *Atmos. Pollut. Res.*, 2021, **12**, 352–364.

59 X.-B. Li, D.-S. Wang, Q.-C. Lu, Z.-R. Peng, S.-J. Lu, B. Li and C. Li, Three-dimensional investigation of ozone pollution in the lower troposphere using an unmanned aerial vehicle platform, *Environ. Pollut.*, 2017, **224**, 107–116.

60 K. Zhang, G. Xiu, L. Zhou, Q. Bian, Y. Duan, D. Fei, D. Wang and Q. Fu, Vertical distribution of volatile organic compounds within the lower troposphere in late spring of Shanghai, *Atmos. Environ.*, 2018, **186**, 150–157.

61 Y. Yan, S. Wang, J. Zhu, Y. Guo, G. Tang, B. Liu, X. An, Y. Wang and B. Zhou, Vertically increased NO_3 radical in the nocturnal boundary layer, *Sci. Total Environ.*, 2021, **763**, 142969.

62 S. Wu, G. Tang, Y. Wang, Y. Yang, D. Yao, W. Zhao, W. Gao, J. Sun and Y. Wang, Vertically decreased VOC concentration and reactivity in the planetary boundary layer in winter over the North China Plain, *Atmos. Res.*, 2020, **240**, 104930.

63 X.-B. Li and G. Fan, Interannual variations, sources, and health impacts of the springtime ozone in Shanghai, *Environ. Pollut.*, 2022, **306**, 119458.

64 G. Tang, X. Zhu, J. Xin, B. Hu, T. Song, Y. Sun, J. Zhang, L. Wang, M. Cheng, N. Chao, L. Kong, X. Li and Y. Wang, Modelling study of boundary-layer ozone over northern China - Part I: Ozone budget in summer, *Atmos. Res.*, 2017, **187**, 128–137.

65 J. Stutz, B. Alicke, R. Ackermann, A. Geyer, A. White and E. Williams, Vertical profiles of NO_3, N_2O_5, O_3, and NO_x in the nocturnal boundary layer: 1. Observations during the Texas Air Quality Study 2000, *J. Geophys. Res.: Atmos.*, 2004, **109**, D12306.

66 X. Cao, W. Chen, H. Du, Y. Hong, J. Lyu, T. Mo, L. Ma, Z. Huang and W. Gao, Remote multi-channel continuous online monitoring system for fugitive emissions of VOCs (In Chinese), *Chin. J. Environ. Eng.*, 2021, **15**, 737–745.